Ultrathin Cellulose Nanofiber Reinforced Ti3C2Tx Crosslinked hydrogel for Multifunctional and Sensitive Sensors

Kangjie Wu
Jiangsu University of Science and Technology
Xiao Chen (xiao_chen@just.edu.cn)
Jiangsu University of Science and Technology
Qing Wang
Jiangsu University of Science and Technology
Xuran Xu
Nanjing University of Science and Technology
Chao Yu
Jiangsu University of Science and Technology
Chuanxiang Chen
Jiangsu University of Science and Technology

Research Article

Keywords: MXene, BCNF, mechanical property, self-healing, hydrogel

Posted Date: December 8th, 2022

DOI: https://doi.org/10.21203/rs.3.rs-2343328/v1

Abstract

Multifunctional strain sensors simultaneously satisfy all the requirements including flexibility, stretchability, biocompatibility and high responsibility to external stimuli are always in high demand for wearable electronics. In this work, we introduced modified bacterial cellulose nanofibers (BCNF) as double network hydrogel-reinforced substrates to prepare MXene-based strain sensor (MPCB). The well-percolated BCNF play important role to reinforce the polymer skeleton and induce the continuous MXene-MXene conductive paths. Consequently, the electrical conductivity was significantly improved and excellent mechanical properties were retained (with the elongation at break over 500%). The prepared hydrogel can act as a wearable sensor for human motion detection, including swallowing movements, finger bending, and wrist bending. They also exhibit promising applications with multiple characteristics, i.e., ideal EMI, adjustable flexibility, self-healing and self-adhesive performance. Our work provides a simple and practical strategy for a new generation of wearable electronic sensor devices.

1. Introduction

With the substantial development of electronic skins and personalized healthcare monitoring technologies, the use of wearable strain sensors has received tremendous attention. (Meng et al., 2022; Li, Zhou, Sarkar, Gagnon-Lafrenais, & Cicoira, 2022; Zhang et al., 2022; Su et al., 2022). As one of the emerging materials, conductive hydrogels have been widely investigated for the preparation of flexible wearable strain sensors (Nie et al., 2022; Zheng et al., 2022) due to their excellent stress-strain adaptability (He et al., 2022; Zhang et al., 2022), tunable mechanical properties, and remarkable biological characteristics (Ye et al., 2022; Yao et al., 2022). Nowadays, hydrogel materials used in strain sensing are increasingly required to meet the diversity of the function, such as a quick and reliable real-time signal response with high and stable conductivity, work efficiently under various conditions, high mechanical performance, strong adhesion to different substrates and easily manipulated (Huang et al., 2022; Yang et al., 2021). Unfortunately, many of the hydrogel-based sensors available today (such as ionic gel, organogel, and composite hydrogels containing conductive nanomaterials) (Li et al., 2022) are unable to adequately satisfy all the requirements listed above. Previous hydrogel systems had some drawbacks, such as poor structural stability, limited mechanical strength and elasticity, unconformable interaction with skin, and a significantly reduced service life. Therefore, it is essential, but also difficult, to create self-adhesive, electrically conductive hydrogel materials using a simple method (Yu et al., 2022; Wang et al., 2022).

In materials science, two-dimensional (2D) sheet-based nanomaterials have already demonstrated interesting and practical potential in various applications including sensing, electronics and optoelectronics. Among them, MXene, as a two-dimensional inorganic substance, has been extensively studied due to its excellent conductivity, good biocompatibility and high hydrophilicity, and is an excellent choice for the preparation of conductive hydrogels (Wang et al., 2021). For example, *Huang et al*. used ammonium polyphosphate (APP) to interact with MXene sheets at the multimolecular level (hydrogen bond, coordination bond, electrostatic), and the conductivity of the synthesized MXene/PAA composite

could reached 8312.4 S cm^{-1} (Huang et al., 2022). However, most of the reported studies focus on the improvement of mechanical or electrical properties, and to some extent ignore other properties that are equally important for practical applications of conductive organic hydrogels, such as adhesion and self-healing properties (Shi et al., 2021). In addition, for the flexible and stretchable hydrogels based on MXene nanosheets, these water-insoluble nanosheets will inevitably aggregate during gelation, leading to serious degradation of the conductive path of the hydrogel network, as well as irreversible damage to the sensor performance. Thus, it is still desirable to further improve the interfacial interaction as well as the versatility of hydrogels, so as to become high performance candidate materials for wearable/stretchable electronics.

Recently, the development of conductive networks with lower electrical conductivity percolation thresholds should prefer supporting or template materials that can establish strong interfacial interaction with conductive fillers, boosting the flexibility and sensitivity (Yang et al., 2022; Qin et al., 2022). For example, *Yang et al*. obtained a highly conductive graphene/polyvinyl alcohol composite by regulating the interfacial interactions, and the conductivity could reach 25 S m^{-1} at the graphene content of only 6.25% (Yang et al., 2019). Combining the advantages of interpenetrating networks, especially for the typical double-network (DN) system, is an effective method to prepare polysaccharide hydrogel sensors, resulting in optimized mechanical properties, self-healing ability and interface adhesion. In search of substrate materials for this purpose, biomass bacterial cellulose nanofiber (BCNF), biologically synthesized by *Acetobacter xylinum*, appears to be an ideal candidate due to the ultra-thin nanofibers (30–50 nm) and unique three-dimensional (3D) interconnected network structure. Such advantages in combination with their higher aspect ratio and higher mechanical strengths have imparted BCNF with unique features that can be harnessed for excellent mechanical enhancement in polymer matrix (Chibrikov et al., 2022; Yang et al., 2021). For instance, *Blaker et al*. prepared self-reinforced PLA composites using only 2 wt% of modified BCNF, which showed a 175% increase in viscoelastic properties in terms of bending storage modulus (Blaker et al. 2014). More attractively, the abundant hydroxyl groups exposed on the surface of the BCNF allow uniformly dispersion and polymerization of monomers along the fibers for the construction of conductive network with high electrical properties. Recently, we have reported the use of BCNF as network pathway construction substrates and reinforcement materials to induce the formation of a nacre MXene-based film with remarkable electrical conductivity (2848 Scm $^{-1}$) (Sun et al., 2021). Therefore, we expect such design of continuous conductive pathways with high aspect ratio and multiple network structure could grantee suitable mechanical properties at low loading of fillers, thus balancing the permeability threshold and strain-sensor behavior obtained.

On the basis of the aforementioned considerations, we used modified bacterial cellulose nanofibers (BCNF) with 30–50 nm diameter as double network hydrogel-reinforced substrates to prepare MXene-based strain sensor. The prepared hydrogel sensor exhibited high stretchability, shape adaptability, adhesion and rapid self-healing ability. The high aspect ratio as well as the strong inter-fiber connections of BCNF fillers are believed to reduce the contact resistance between organic-inorganic interfaces, and simultaneously endow the formation of more efficient mechanical interlocking. Therefore, a tightly

packed 2D/1D structure was built in PVA matrix with well-percolated BCNF/PVA reinforcing skeleton and continuous MXene-MXene conductive paths. As a result, over a strain range of more than 250%, a measurement factor of 46.64 can be achieved, which is much better than most reported MXene-based stretchable strain sensors. The MPCB sensors thus have been shown to be useful in a variety of wearable motion monitoring ranges, including finger movements, elbow bending, and knee bending. Moreover, the sensor also exhibits multiple characteristics, i.e., ideal EMI, tunable flexibility, self-healing and self-adhesive performance, indicating its tremendous potential applications in future intelligent electronics.

2. Experimental

2.1 Materials

Ti_3AlC_2 was supplied by Yiyi Technology Co., Ltd. 2,2,6,6-tetramethylpiperidine-1-oxyl (TEMPO, 98%), sodium hypochlorite (NaClO, 99%), sodium chlorite (NaClO , 98%), ethanol (99.5%), lithium fluoride (LiF, 99.9%), hydrochloric acid (HCl, 36%), polyvinyl alcohol (PVA, Mw ~ 47,000), sodium tetraborate (≥ 99%) were obtained from Aladdin Reagent (Shanghai) Co., LTD. Sulfuric acid (H_2SO_4, 98%) was obtained from Sinopharm Chemical Reagent Co. LTD. Polyethylene glycol (PEG, Mw 4000) was obtained from Tianjin Sinoopod Technology Co., LTD. All chemicals were used as received without further purification.

2.2 Preparation of highly dispersible BCNF

Following a dynamic fermentation process at 30°C, raw BC were grown utilizing an *Acetobacter xylinum NUST4.2* as previously reported (Yan et al. 2017). The sample was then treated with 0.1% sodium hydroxide solution and hydrogen peroxide for 6 h at 80°C and was then thoroughly rinsed with distilled water. Afterwards, 2.0 g of prefabricated BC was mixed with 200 mL of PBS buffer (0.05 M, pH 6.8) and agitated at 60°C for 30 minutes in a flask. Then TEMPO (0.036 g, 0.2 mmol), $NaClO_2$ (3 mmol) and NaClO (30 mmol) were added and the solution was agitated for 24 hours at 60°C. After quenching the TEMPO oxidation with 10 mL of ethanol, the TEMPO-oxidized BC was obtained by washing and repeated centrifugation. The final step involved homogenizing the diluted products (0.5 wt%) were obtained at pressures of 100 MPa for up to 30 HPH cycles in a high-pressure homogenizer (AH-2010, ATS Engineering Inc., Canada).

2.3 Preparation of MXene nanosheet layers

MXene nanosheets were obtained by selectively etching Al in Ti_3AlC_2. 1.0 g of Ti_3AlC_2 was added to 20 ml of hydrochloric acid solution containing 1.0 g of LiF (6 M). Then magnetically stirred at 35°C for 24 h, the resulting suspension was washed with distilled water and centrifuged several times at 6000 rpm to give clay-like $Ti_3C_2T_x$ granules. Subsequently, the pellet was dispersed in deionized water and sonicated for 3 h to obtain a layered $Ti_3C_2T_x$ nanosheet, named MXene. MXene samples were collected by centrifugation, freeze-dried for 24 h, and the MXene suspension was prepared with water at a content of 0.5 wt% for subsequent experiments.

2.4 Preparation of MPCB conductive hydrogels

First, 0.01 g of PEG was added to the appropriate amount of MXene suspension as solution A. Meanwhile, 5 ml of 10% PVA solution was added to the appropriate amount of BCNF suspension as solution B. After well dispersed, solution B was slowly dripped into solution A under vigorous stirring. The mixture was gradually gelated through the addition of 2 mL of aqueous sodium tetraborate solution (5 wt%) under vigorous agitation. The gel was subsequently transferred to a fixed size mold (2 cm×1 cm×0.5 cm). The final sample was obtained after repeated freeze (-17 ℃) and thaw cycles and named as MPCB. Different samples were prepared for comparison, including the MXene solid content of 0, 15 mg, 30 mg, 45 mg, 60 mg, 75 mg, respectively, with the constant BCNF content of 20 mg, and the BCNF solid content of 0,10 mg, 20 mg, 30 mg, 40 mg, 50 mg, respectively with the constant MXene content of 30 mg. Samples without BCNF were also prepared and named as MXene/PVA-B. The detailed characterization of hydrogels was described in Support Information.

3. Results And Discussion

3.1. Design, synthesis and structural characterizations of the MPCB hydrogels

The structure and formation mechanism of the organohydrogel is illustrated in Fig. 1a. So far, due to the lack of interface compatibility between MXene nanosheets and hydrogel components, the rational design of signal recognition system is still faced with challenges (Park et al. 2021). In our work, the modified BCNF was employed to construct and reinforce continuous conductive network for the preparation of MXene-based sensing material. To improve the reinforce performance of BCNF fillers, a TEMPO-oxidation treatment accompanied with high-pressure homogenization was firstly carried out. Afterwards, a more uniform and clear solution was obtained compared to the origin BC solution as shown in Figure S1a. The prepared BCNF maintain an ultrathin conformation with a thickness of only 30–50 nm (Figure. S1b), which is expected to facilitate the formation of continues network in polymer matrix. The electrostatic repulsion between carboxyl groups on BCNF is beneficial to improve their dispersity in polymer matrix, and the abundant hydroxyl groups present high affinity for other components, rending the excellent stability as well as dispersibility for BCNF during the subsequent preparation of hybrid hydrogels. Subsequently, MXene nanosheets prepared from the Ti_3AlC_2 (MAX) precursor were added to the mixture solution. The morphology characterization shown in Figure. 1b and 1c confirm large dimension with a diameter of only 4.2 nm for the delaminated MXene nanosheets. Benefiting from the abundant hydrophilic functional groups (-OH, -F, -O, etc.) on the surface of MXene nanosheets, they can be well dispersed in BCNF/PVA dual network system, forming a continuously conductive network entangled with the polymer chains. Subsequently, borax was applied to the gelation of MXene/BCNF/PVA solution to form a self-healing network with dynamic reversible effect. The formation of the dynamic cross-linking of didiol-borax complexation as well as hydrogen bonding between the hydroxyl groups on BCNF/PVA chains results in abundant reversible hydrogen bonds and supramolecular interactions in the obtained

organohydrogels (Wang et al. 2022). The MPCB hydrogels with ideal injectability, shapeability as well as stretchability, were finally obtained via a freezing-thawing cycle process (Fig. 1d).

We first examined the morphologies of the MXene/PVA-B and MPCB hydrogels by SEM. Figure 2a and 2b show a dense fracture surface with mountain-like structure of the MXene/PVA-B samples, in which one can see obvious agglomeration of the 2D and polymer matrix (Qin et al. 2022). Compared to the samples without BCNF, our MPCB hydrogels exhibited a honeycomb porous structure as shown in Fig. 2c and 2d, implying the important role of BCNF in the formation of continues dual network system. Noticeably, a distinct polymer-fiber dual network structure can be observed with the homogeneous distribution of MXene nanosheets in the system, which was confirmed by by EDS spectroscopy in Fig. 2e. The elemental distribution of Ti was about 5.1%. We believed that the integration of enriched hydrogen bonds and covalent interactions with MXene nanosheets into the polymer network could ensure a more robust, compact, and homogeneous cross-linked network, thus promoting the strain sensing performance. The chemical structure of PVA, BCNF, MXene, MPCB samples was detected by FT-IR, and the spectra are shown in Figure S4a. Both PVA and BCNF have a common peak around 3300 cm^{-1}, which corresponds to the telescopic vibration of the hydroxyl group (Kim et al. 2019). Meanwhile, the peaks observed at 2900, 1417, and 1029 cm^{-1} are attributed to the stretching, bending and rocking modes of C-H bonds, respectively (Yuan et al. 2022), further confirming the interactions between PVA and BCNF in MPCB hydrogels. The crystalline structures of the samples were investigated by XRD and the results are shown in Figure S4b. It is found that the peaks of 2θ = 22.8◦ and 14.8◦ represent the (200) and (110) planes in cellulose I, while the single strong peak of 2θ = 20.4° corresponds to the PVA diffraction pattern. (Xu et al. 2021). To confirm that MXene is included in the hydrogel network, we perform X-ray photoelectron spectroscopy (XPS) spectroscopy on MPCB hydrogels. The XPS spectrum (Figure S4c) shows the presence of F, O, Ti, and C elements in the hydrogel, indicating that MXene successfully doped into the MPCB hydrogel. The high resolution C1s XPS spectra of MPCB hydrogel are shown in Figure. S4d. The peaks in the C1s spectrum at 281.23, 284.63, 286.33 and 288.08 eV were indicative of Ti-C, C-C, C-O and O-C = O, respectively (Wang et al. 2020).

3.2. Conductive and Mechanical properties

It is proved that the intrinsic conductivity of strain sensors is one of the critical factors to determine their strain sensing performance. In our work, based on the excellent rigidity characteristics and skeleton function of BCNF, the design of dual-network structure is believed to be beneficial to enhance the conductive pathway constructed by MXene (Khodami et al., 2022). This architecture could induce more low-defect and high-efficiency electronic channels, thus resulting in excellent conductivity and ideal strain sensing performance. To investigate this function, we fist compared the electrical conductivity of MPCB hydrogels with different BCNF contents under fixed MXene content. For the blank sample, the conductivity of MPCB was found to be 5.32×10^{-5} S cm^{-1}. Interestingly, this value significantly increased with the increase of BCNF content and finally reached the maximum value of 1.77×10^{-3} S cm^{-1} at the content of 30 mg BCNF. The phenomenon was attribute to the addition of proper amount of BCNF can effectively promote the construction of double network structure in polymer matrix, thus inducing MXene

to form continuous conductive pathway with better dispersion in the system. Afterwards, excess BCNF inhibit the growing trend due to their intrinsic insulating properties. The adsorbed BCNF on the surface of nanosheets may hinder their contact and lower the conductivity.We also investigate the effect of different MXene content on the conductivity of MPCB hydrogel as shown in Fig. 3b. Obviously, the increase of conductive filler plays obvious promoting effect on the conductivity of the material, and this trend showed a dramatic increase was when the MXene content changed from 30 mg to 45 mg, and this trend gradually slowed down with the further increasing of MXene content.

Next, we evaluated the mechanical properties of different samples under varying BCNF and MXene contents. As shown in Fig. 3c and 3d, the addition of BCNF can significantly improve the mechanical strength of nanocomposites, but the ductility is significantly decreased. (Chhetri et al. 2022). The tensile strength rose from 30.8 kPa to 105.5 kPa with the elongation at break drastically decreasing from 1432.0–591.9%. Correspondingly, the compressive performance was greatly improved from 66.5 kPa to 469.3 kPa when the compression degree reached 80%. Noticeably, a significant gradient can be found with the content of BCNF exceeding to 20 mg, which may cause a negative impact on the sensing performance with lower tensile strain properties. Meanwhile, the influence of MXene content on the the mechanical properties of MPCB hydrogels was evaluated and the results are shown in Fig. 3e and 3f. We found that the positive effect on tensile strain strength with increase of MXene content is less than that of BCNF, but the influence trend on elongation at break is similar to that of BCNF. When the MXene content increased from 45 mg to 60 mg, the elongation at break decreased significantly from 1010.7–508.7%, while the tensile strain strength did not increase significantly. It was speculated that excessive MXene caused local stacking in the MPCB network structure, which greatly affected the tensile modulus of the material, resulting in significant performance degradation. Therefore, the optimal composite ratio of the material was chosen as the BCNF content of 20 mg and MXene content of 45 mg for subsequent performance studies.

3.3. Rheological properties

We subsequently performed a series of rheology measurements to investigate the viscoelasticity and ductility led by the incorporation of BCNF and MXene into the PVA-based hydrogels. The values of G', G", and η* in the ω range of 0.1–100 rad s^{-1} for the hydrogels under different contents of reinforcers are illustrated in Fig. 4. One can see that regardless of the hydrogel composition, all three characters showed an apparent change as a function of increasing ω, which is consistent with previous studies of other PVA based composites (Wang et al. 2020). In the low frequency region, the samples mainly exhibit liquid properties due to the reversible cross-link of the network. As ω increases, it was found that the value of G' gradually approaches G "and then is 2 times higher than G", because the unstable cross-links do not have enough time to dissociate at higher ω. In this situation, the difference between G' and G" is getting larger and hydrogels exhibit elastic-like behavior (Prasser et al. 2022). Moreover, as can be seen from the changes in Fig. 4cf and S5, the variation trends of G* and η* of hydrogels under different MXene and BCNF contents were similar. It should be pointed out that the effect of increasing BCNF content on the

above characters is 2–3 times that of increasing the content of MXene filler, further confirming role of BCNF in enhancing the mechanical properties of 3D networks. Meanwhile, one can also see the increase of MXene content leads to the decrease of viscoelastic properties because the presence of MXene would lead to the consumption of borate,. In this view, the existence of one-dimensional BCNF reinforcing filler and two-dimensional MXene conductive filler bring adjustable diversity and difference to PVA matrix. By adjusting the amounts of different fillers, especially the content of BCNF, the viscoelastic properties can be easily adjusted according to the actual application requirements.

3.4. Sensing propertie

Due to the excellent performance of MPCB composite hydrogel in electrochemical and mechanical properties, combined with the good biocompatibility characteristics of PVA/BCNF substrate, it is expected to function as a wearable tensile strain sensing material for monitoring human movement behavior. To do this, we embedded the fixed fine copper wires at each end of the MPCB for the collection of resistance signals. The sensing performance test was then carried out within an appropriate tensile range (0-250%). The tensile strain rate (%) and $\Delta R/R_0$ were used to express the resistance change of the material during continuous stretching, and the ratio of the two (gauge factor, GF) was used to express the sensing sensitivity of the material. From the results in Fig. 5a, we can see the curve can be fitted to four linear regions and the linearities show increasing slope: the linear range of 0 to 121% was 0.99, the linear range of 121 to 218% was 0.97, the linear range of 219 to 237% was 0.99, and the linear range of 238 to 250% was 0.97. The gauge factor of the corresponding linear region was 0.94, 3.68, 12.04, and 46.64, respectively. It is assumed that the interfacial interactions between the conductive pathway and polymer based dual network inhibit crack propagation and thus multiply the working strain range. A literature comparison study was also presented in Table. S1, one can see that our fabricated MPCB strain sensor has a wider response range and superior sensitivity compared to most reported polysaccharide based strain sensors.

We further investigate the variation of $\Delta R/R_0$ under different cyclic strains including 250, 150 as well as 50%. As shown in Fig. 5b, the MPCB sensor presented excellent stability during multiple stretching cycles, with corresponding $\Delta R/R_0$ values of 15.5, 3.2 and 1.5, respectively. Next, the feasibility of our MXene-based hydrogel served as stress-strain sensor was verified by monitoring various human movements, including the motion of swallowing, finger, and elbow (Figure. 5c-5e). Firstly, one can see that under a low strain such as the motion of Adam's apple of a man, the electrical signal outputs deriving from the movement are quite stable and repeatable. As the strain range gradually increases, such as finger bending and knee bending, the repeatability of the signal can also be kept within an acceptable error range. Meanwhile, with the release of all the actions, the signals accordingly return to its original values, revealing the excellent sensitivity and good repeatability of our sensors.

3.5. Self-healing and adhesive performance

Self-healing and self-adhesiveness are two important advantages of conductive hydrogels, because self-healing can significantly extend the service life of organic hydrogels and self-adhesiveness is crucial to interface connection, thus satisfying the needs of different application environments. To corroborate this, the self-healing experiments were first conducted and the results are shown in Fig. 6a-6d. We can see the prepared MXnene-based hydrogel could be self-healed in several seconds without any external stimulation even under stretching force. Additionally, we conducted tensile strain test on the self-healing material and found that the tensile strain curve of the material was basically consistent with the original material, with a slight decrease of tensile strength and elongation at break compared to the original material (Fig. 6e). In addition, the conductivity of the hydrogel exhibited similar values to the original (maintained at 2.10 S/m) for several cut-healing cycles, revealing interesting self-healing properties (Fig. 6f). The microscopic morphological changes at the healing site were also investigated by SEM as shown in Fig. 6g, in which one can see the clear interconnection between the cutting edges, confirming the ideal self-healing properties. Compared to the origin sample, which can maintain good flexibility and ductility under severe mechanical deformation, such as twisting at 720° and stretching at 300% (Fig. 6h), the healed samples could still preserve excellent ductility as shown in Fig. 6i.

We further applied the hydrogels as conductor in a circuit comprising a light-emitting diode (LED) lamp and 1.5 V constant voltage. Firstly, one can see the LED lamp was successfully lit in this hydrogel based conductor circuit. It is striking that the lamp could still remain brightness even under stretch of 500% deformation of the hydrogel conductor (Fig. 7ai-iii). Once cutting off the hydrogel, the light of lamp was immediately switched off (Fig. 7a-iv). As expected, the LED light can be relit with barely changed when the fractured parts are manually recontacted, due to the strong hydrogen bonds and the restoration electrical pathway (Fig. 7a-v). Noticeably, the healed hydrogel could still be stretched to ~ 50% while maintaining the brightness of the lamp, indicating its good healing capacity for strain sensing (see Fig. 7a-vi). The corresponding schematic diagrams of the circuit during the healing process is presented in Fig. 7b. In addition, due to the abundant number of hydrogen bonds in the hydrogel, the sample ensures impressively good adhesion to many different substrates such as metal, glass, synthetic rubber, and paper (Fig. 7d). The adhesive performance can be remained at a high level even after undergoing a relatively long-time exposure of 14 days, as displayed in Figure S6. Since it is reported that 1D cellulose nanofiber could greatly reduce the contact resistance between overlapped MXene planes, thus thus greatly improving the mechanical properties while maintaining high electrical conductivity (Xu et al. 2021). Therefore, the prepared hydrogels are also expected to be applied to other functions, such as obtaining excellent electromagnetic interference properties. As shown in Figure. 7c, with increasing the content of MXene from 0 to 60 mg, the EMI SE increases obviously at the frequency ranging from 8.2 to 12.4 GHz (X-band). When the content of MXene was 60 mg, the EMI SE could reach 43.5 dB, which was higher than that of most previous reported MXene composite material (Table S2), demonstrated excellent protective performance as a wearable device. It is envisioned that the MPCB hydrogels exhibit promising applications for flexible wearable sensors with multiple characteristics, i.e., good electrical conductivity, ideal EMI, tunable flexibility, self-healing and self-adhesive performance.

4. Conclusion

In summary, we have reported the construction of a multifunctional strain sensor based on 2D MXene conductive filler in a dual polymer network. The well-percolated BCNF with strong interfacial interactions was employed to reinforce the polymer skeleton and induce the continuous MXene-MXene conductive paths. Consequently, at a MXene loading of only 20 mg, the conductivity of the hydrogel was significantly improved without sacrificing its mechanical properties (maintain the elongation at break over 500%). A gauge factor of 46.64 over a strain range of more than 250% could be achieved, which is significantly better than most reported MXene-based stretchable strain sensors. In addition, the MPCB sensor is proven to be adopted in a variety of wearable motion monitoring ranges, including finger movements, elbow bending, and knee bending. Meanwhile, the MPCB hydrogels exhibit multiple characteristics, including ideal EMI property, tunable flexibility, self-healing as well as self-adhesive performance. Therefore, this study provides a simple and scalable way to construct an effective conductive network in elastic strain sensors that can be used for a wide range of applications, facilitating the development of biomaterial-based sensors in flexible electronic devices.

Declarations

Declaration of competing interest

There are no conflicts to declare in this paper.

Acknowledgement

The authors thank the financial support from the National Natural Science Foundation of China (52003121), the Natural Science Foundation of Jiangsu Province (BK20210357) and the China Postdoctoral Science Foundation (2020M671497, 2020T130300).

Authors' contributions

Kangjie Wu: Investigation, Formal analysis; Writing;

Xiao Chen: Investigation, Data Curation, Writing, Supervision;

Qing Wang: Investigation;

Chao Yu: Validation;

Xuran Xu: Methodology, Formal analysis;

Chuanxiang Chen: Visualization;

Data availability

All data generated during this study are included in this published article.

References

1. Azadi, S., Peng, S., Moshizi, S. A., Asadnia, M., Xu, J., Park, I., et al. (2020) Biocompatible and highly stretchable PVA/AgNWs hydrogel strain sensors for human motion detection. *Adv. Mater. Technol*, *5(11)*, 1-12.
2. Bai, Y., Bi, S., Wang, W., Ding, N., Lu, Y., Jiang, M., et al. (2022). Biocompatible, stretchable, and compressible cellulose/MXene hydrogel for strain sensor and electromagnetic interference shielding. *Soft Materials*, DOI: 10.1080/1539445X.2022.2081580.
3. Blaker, J., Lee, K., Walters, M., Drouet, M., Bismarck, A. (2014). Aligned unidirectional PLA/bacterial cellulose nanocomposite fibre reinforced PDLLA composites. *React Funct Polym*, *85*, 185-192.
4. Chherti, K., Subedi, S., Muthurasu, A., Ko, T., Dahal, B., Kim, H. (2022). A review on nanofiber reinforced aerogels for energy storage and conversion applications. *J Energy Storage*, *46*, 103927.
5. Chen, Y., Lu, K., Song, Y., Yue, Y., Wu, Q., & Xiao, H. (2019). A Skin-Inspired Stretchable, Self-Healing and Electro-Conductive Hydrogel with A Synergistic Triple Network for Wearable Strain Sensors Applied in Human-Motion Detection. *Nanomaterials*, *9*, 1737.
6. Chibrikov, V., Pieczywek, P, M., & Zdunek, Artur. (2022). Tailor-Made Biosystems - Bacterial Cellulose-Based Films with Plant Cell Wall Polysaccharides. *Polym Rev (Phila Pa)*, 2067869.
7. Gu, J., Huang, J., Chen, G., Hou, L., Zhang, J., Zhang, X., et al. (2020) Multifunctional poly(vinyl alcohol) nanocomposite organohydrogel for flexible strain and temperature sensor. *ACS Appl. Mater*, *12*(36), 40815-40827.
8. Huang, J., Wu, P. (2022). Kneading-Inspired Versatile Design for Biomimetic Skins with a Wide Scope of Customizable Features. *Adv. Sci*., *9(14)*, 1-9.
9. He, X., Dong, J., Zhang, X., Bai, X., Zhang, C., Wei, D., (2022). Self-Healing, Anti-Fatigue, antimicrobial ionic conductive hydrogels based on Choline-Amino acid polyionic liquids for Multi-Functional sensors. *Chem. Eng. J*., *435*, 135168.
10. Huang, X., Huang, J., Zhou, G., Wei, Y., Dong, A., & Yang, D. (2022). Gelation-Assisted Assembly of Large-Area, Highly Aligned, and Environmentally Stable MXene Films with an Excellent Trade-Off between Mechanical and Electrical Properties. *Small*, *18*, 2200829.
11. Huang, J., Zhao, M., Cai, Y., Zimniewska, M., Li, D., & Wei, Q. (2020). A Dual-Mode Wearable Sensor Based on Bacterial Cellulose Reinforced Hydrogels for Highly Sensitive Strain/Pressure Sensing. *ADV ELECTRON MATER*, *6(1)*, 1900934.
12. Huang, C., Luo, Q., Miao, Q., He, Z., Fan, P., Chen, Y., et al. (2022). MXene-based double-network organohydrogel with excellent stretchability, high toughness, anti-drying and wide sensing linearity for strain sensor. *Polymer*, *253*, 124993.
13. Jin, L., Wang, P., Cao, W., Song, N., & Ding, P. (2022). Isolated Solid Wall-Assisted Thermal Conductive Performance of Three-Dimensional Anisotropic MXene/Graphene Polymeric Composites. *ACS Appl.*

Mater., *14*, 1747-1756.

14. Jiang, Y., Ru, X., Che, W., Jiang, Z., Chen, H., Hou, J., et al. (2022). Flexible, mechanically robust and self-extinguishing MXene/wood composite for efficient electromagnetic interference shielding. *COMPOS PART B-ENG*, *229*, 109460.
15. Khodami, S., Kaniewska, K., Stojek, Z., Karbarz, M. (2022). Hybrid double-network dual-crosslinked hydrogel with self-healing ability and mechanical stability. Synthesis, characterization and application for motion sensors. *EUR POLYM J*, *173*, 111258.
16. Kim, J., Park, H., Lee, G., Yoon, J., Kim, M., Ha, J. (2019). Paper-Like, Thin, Foldable, and Self-Healable Electronics Based on PVA/CNC Nanocomposite Film. *Adv. Funct. Mater.*, 1905968.
17. Li, Y., Zhou, X., Sarkar, B., Gagnon-Lafrenais, N., & Cicoira, F. (2022). Recent Progress on Self-Healable Conducting Polymers. *Adv. Mater.*, *34*, 2108932.
18. Li, W., Zhang, J., Niu, J., Jin, X., Qian, X., Xiao, C., et al. (2022). Self-powered and high sensitivity ionic skins by using versatile organogel. *Nano Energy*, *99*, 107359.
19. Li, G., Huang, K., Deng J., Guo M., Cai M., Zhang Y., et al. (2021). Highly conducting and stretchable double network hydrogel for soft bioelectronics. *Adv. Mater.*, *34(35)*, 2200261.
20. Lu, Y., Qu, X., Zhao, W., Ren, Y., Si, W., Y., & Wang, W. (2020). Highly Stretchable, Elastic, and Sensitive MXene-Based Hydrogel for Flexible Strain and Pressure Sensors.*Research*, *2020*, 2038560.
21. Luo, X., Zhu, L., Wang, Y., Li, J., Nie, J., Wang, Z. (2021). A Flexible Multifunctional Triboelectric Nanogenerator Based on MXene/PVA Hydrogel. *Adv. Funct. Mater.*, *31(38)*, 1-9.
22. Li, X., He, L., Li, Y., Chao, M., Li, M., Wan, P., & Zhang, L. (2021). Healable, Degradable, and Conductive MXene Nanocomposite Hydrogel for Multifunctional Epidermal Sensors. *ACS Nano*, *15(4)*, 7765–7773.
23. Liu, S., Li, D., Wang, Y., Zhou, G., Ge, K., & Fang, D. (2022). Flexible, high-strength and multifunctional polyvinyl alcohol/MXene/polyaniline hydrogel enhancing skin wound healing. *Biomater. Sci*, DOI: 10.1039/d2bm00575a.
24. Liu, J., Zhang, Y., Cheng, W., Lei, S., Song, L., Hu, Y., et al. (2022). Anti-Fogging, Frost-Resistant transparent and flexible silver Nanowire-Ti3C2Tx MXene based composite films for excellent electromagnetic interference shielding ability. *J. Colloid Interface Sci.*, *608*, 2493–2504.
25. Liu, D., Gao, Y., Song, Y., Shi, H., Yang, Q., & Xiong, C. (2022). Highly Sensitive Multifunctional Electronic Skin Based on Nanocellulose/MXene Composite Films with Good Electromagnetic Shielding Biocompatible Antibacterial Properties. *Biomacromolecules*, *23*, 182-195.
26. Meng, K., Wei, W., Chen, G., Shen, S., Xiao, X., & Chen, J. (2022). Wearable Pressure Sensors for Pulse Wave Monitoring. *Adv. Mater.*, *34*, 2109357.
27. Nie, Y., Yue, D., Xiao, W., Wang, W., Chen, H., Bai, L., et al. (2022). Anti-freezing and self-healing nanocomposite hydrogels based on poly(vinyl alcohol) for highly sensitive and durable flexible sensors. *Chem. Eng. J.*, *436*, 135243.

28. Park, D., Kim, J., Shin, K., Kim, J. (2021). Bacterial cellulose nanofibrils-reinforced composite hydrogels for mechanical compression-responsive on-demand drug release. *Carbohydrate Polymers*, *272*, 118459.
29. Prasser, Q., Steinbach, D., Münch, A., Neubert, R., Mertens, F., & Plamper, F. (2022). Interfacial Rearrangements of Block Copolymer Micelles Toward Gelled Liquid–Liquid Interfaces with Adjustable Viscoelasticity. *Small*, *18*, 2106956.
30. Qin, Y., Mo, J., Liu, Y., Zhang, S., Wang, J., Fu, Q. (2022). Stretchable Triboelectric Self-Powered Sweat Sensor Fabricated from Self-Healing Nanocellulose Hydrogels. *Adv. Funct. Mater.*, 2201846.
31. Qiu, W., Chen, G., Zhu, H., Zhang, Q., Zhu, S. (2022). Enhanced stretchability and robustness towards flexible ionotronics via double-network structure and ion-dipole interactions. *Chem. Eng. J.*, *43*, 134752.
32. Qin, R., Li, X., Hu, M., Shan, G., Seeram, R., Yin, M. (2022). Preparation of high-performance MXene/PVA-based flexible pressure sensors with adjustable sensitivity and sensing range. *Sens. Actuator A Phys.*, *338*, 113458.
33. Qin, M., Yuan, W., Zhang, X., Wei, Y., Chen, W., Huang, D., et al. (2022). Preparation of PAA/PAM/MXene/TA hydrogel with antioxidant, healable ability as strain sensor. *COLLOID SURFACE B*, *214*, 112482.
34. Su, T., Liu, N., Lei, D., Wang, L., Ren, Z., Su, J., et al. (2022). Flexible MXene/Bacterial Cellulose Film Sound Detector Based on Piezoresistive Sensing Mechanism. *ACS Nano*, *16*, 8461–8471.
35. Song, M., Yu, H., Zhu, J., Ouyang, Z., Abdalkarim, S. Y., Tam, K. C., et al. (2020). Constructing stimuli-free self-healing, robust and ultrasensitive biocompatible hydrogel sensors with conductive cellulose nanocrystals. *Chem. Eng. J*, *398*, 125547.
36. Shi, N., Zhi, R., Bi, F., Li, Z., Joonho, B., Long, C. (2021). Environmentally stable, mechanically flexible, self-adhesive, and electrically conductive Ti3C2TX MXene hydrogels for wide-temperature strain sensing. *Nano Energy*, *90*, 106502.
37. Wang, Z., Han, X., Wang, S., Han, X., & Pu, J. (2021). MXene/wood-based composite materials with electromagnetic shielding properties. *Holzforschung*, *75(5)*, 494–499.
38. Wang, J., Li, Q., Li, K., Sun, X., Wang, Y., Zhuang, T., et al. (2022). Ultra-High Electrical Conductivity in Filler-Free Polymeric Hydrogels Toward Thermoelectrics and Electromagnetic Interference Shielding. *Adv. Mater.*, *34(12)*, 1-14.
39. Wang, M., Feng, X., Wang, X., Hu, S., Zhang, C., & Qi, H. (2021). Facile gelation of a fully polymeric conductive hydrogel activated by liquid metal nanoparticles. *J. Mater. Chem. A*, *9*, 24539.
40. Wang, X., Wang, X., Yin, J., Zhang, L., Qin, Z., Jiao, T., et al. (2022). Mechanically robust, degradable and conductive MXene-composited gelatin organohydrogel with environmental stability and self-adhesiveness for multifunctional sensor. *Composites Part B*, *241*, 110052.
41. Wang, Y., Liu, S., Wang, Q., Fu, X., Fatehi, P. (2020). Performance of polyvinyl alcohol hydrogel reinforced with lignin-containing cellulose nanocrystals. *Cellulose*, *27*, 8725-8743.

42. Wang, Z., Zhou, Z., Wang, S., Yao, X., Han, X., Cao, W., et al. (2022). An anti-freezing and strong wood-derived hydrogel for high-performance electronic skin and wearable sensing. *Compos. B. Eng*, *239*, 109954.
43. Wang, Y., Zhang, L., & Lu, A. (2020). High stretchable, transparent cellulose/PVA composite hydrogel for multiple sensing and triboelectric nanogenerator. *J. Mater*, *8*, 13935-13941.
44. Wang, C., Shen, Z., Hu, P., Wang, T., Zhang, X., Liang, L., et al. (2022). Facile fabrication and characterization of high-performance Borax-PVA hydrogel. *J Solgel Sci Technol*, *101*(1), 103-113.
45. Xin, W., Xi, G., Cao, W., Ma, C., Ma, M., & Bian, J. (2019). Lightweight and flexible MXene/CNF/Silver composite membranes with a brick-like structure and high-performance electromagnetic interference shielding. *RSC Adv*, *9*, 29636.
46. Xu, X., Wu, S., Cui, J., Yang, L., Wu, K., Chen, X., et al. (2021). Highly stretchable and sensitive strain sensor based on polypyrrole coated bacterial cellulose fibrous network for human motion detection. *Compos. B. Eng*, *211*, 108665.
47. Xu, X., Wu, S., Cui, J., Yang, L., Liu, D., Wu, K., et al. (2020). Insights into the microstructures and reinforcement mechanism of nano-fibrillated cellulose/MXene based electromagnetic interference shielding film. *Cellulose*, *28*, 3311–3325.
48. Ye, Y., Jiang, F. (2022). Highly stretchable, durable, and transient conductive hydrogel for multi-functional sensor and signal transmission applications, *Nano Energy*, *99*, 107374.
49. Yao, X., Zhang, S., Qian, L., Wei, N., Valentin N., Sergiu C. (2022). Super Stretchable, Self-Healing, Adhesive Ionic Conductive Hydrogels Based on Tailor-Made Ionic Liquid for High-Performance Strain Sensors. *Adv. Funct. Mater.*, *2204565*, 1-14.
50. Yu, X., Zhang, H., Wang, Y., Fan, X., Li, Z., Zhang, X. (2022). Highly Stretchable, Ultra-Soft, and Fast Self-Healable Conductive Hydrogels Based on Polyaniline Nanoparticles for Sensitive Flexible Sensors. *Adv. Funct. Mater.*, *2204366*, 1-11.
51. Yan, G., He, S., Ma, S., Zeng, A., Chen, G., Tang, X., et al. (2021). Catechol-based all-wood hydrogels with anisotropic, tough, and flexible properties for highly sensitive pressure sensing. *Chem. Eng. J.*, *427*, 131896.
52. Yang, M., Cheng, Y., Yue, Y., Chen, Y., Gao, H., Li, L., et al. (2022). High-Performance Flexible Pressure Sensor with a Self-Healing Function for Tactile Feedback. *Adv. Sci.*, *2200507*, 1-11.
53. Yang, L., Weng, W., Fei, X., Pan, L., Hu, Z., Zhu, M. (2019). Revealing the Interrelation between Hydrogen Bonds and Interfaces in Graphene/PVA Composites towards Highly Electrical Conductivity. *Chem. Eng. J.*, *383*, 123126.
54. Yang, Z., Huang, R., Zheng, B., Du, Y., Wu, D., Wang, H., et al. (2021). Highly Stretchable, Adhesive, Biocompatible, and Antibacterial Hydrogel Dressings for Wound Healing. *Adv. Sci.*, *8*, 2003627.
55. Yang, L., Cui, J., Zhang, L., Xu, X., Chen, X., Sun, D. (2021). A Moisture-Driven Actuator Based on Polydopamine Modified MXene/Bacterial Cellulose Nanofiber Composite Film. *Adv. Funct. Mater.*, *27(31)*, 2101378.

56. Yuan, K., Li, X., Yang, X., Luo, S., Yang, X., Guo, Y. (2022). Effect of bacterial cellulose nanofibers incorporation on acid-induced casein gels: microstructures and rheological properties. *Int. J. Food Eng.*, *18(1)*, 41–51.
57. Zhang, Y., Yang, J., Hou, X., Li, G., Bai, N.,Cai, M., et al. (2022). Highly stable flexible pressure sensors with a quasi-homogeneous composition and interlinked interfaces. *Nat. Commun*, *13*, 1317.
58. Zheng, H., Chen, M., Sun, Y., Zuo, B., (2022). Self-Healing, Wet-Adhesion silk fibroin conductive hydrogel as a wearable strain sensor for underwater applications. *Chem. Eng. J.*, *446*, 136931.
59. Zheng, H., Chen, M., Sun, Y., Zuo, B., (2022). Self-Healing, Wet-Adhesion silk fibroin conductive hydrogel as a wearable strain sensor for underwater applications. *Chem. Eng. J.*, *446*, 136931.
60. Zhang, Y., Ren, E., Li, A., Cui, C., Guo, R., Tang, H., et al. (2021) A porous self-healing hydrogel with an island-bridge structure for strain and pressure sensors. *J Mater Chem B*, *9(3)*, 719-730.
61. Zhang, J., Wan, L., Gao, Y., Fang, X., Lu, T., Pan, L., et al. (2019) Highly stretchable and self-healable MXene/Polyvinyl alcohol hydrogel electrode for wearable capacitive electronic skin. *Adv. Electron. Mater.*, *5(7)*, 1-10.
62. Zeng, Z., Yu, S., Guo, C., Lu, D., Geng, Z., & Pei, D. (2022). Mxene Reinforced Supramolecular Hydrogels with High Strength, Stretchability, and Reliable Conductivity for Sensitive Strain Sensors. *Macromol. Rapid Commun*. 2200103.
63. Zhang, Y., Mao, J., Jiang, W., Wei, G., Zuo, M., Ni, Y., et al. (2021). Lignin sulfonate induced ultrafast polymerization of double network hydrogels with anti-freezing, high strength and conductivity and their sensing applications at extremely cold conditions. *COMPOS PART B-ENG*, *217*, 108879.
64. Zhou, Y., Fei, X., Tian, J., Xu, L., Li, Y. (2022). A ionic liquid enhanced conductive hydrogel for strain sensing applications. *J. Colloid Interface Sci.*, *606*, 192–203.

Figures

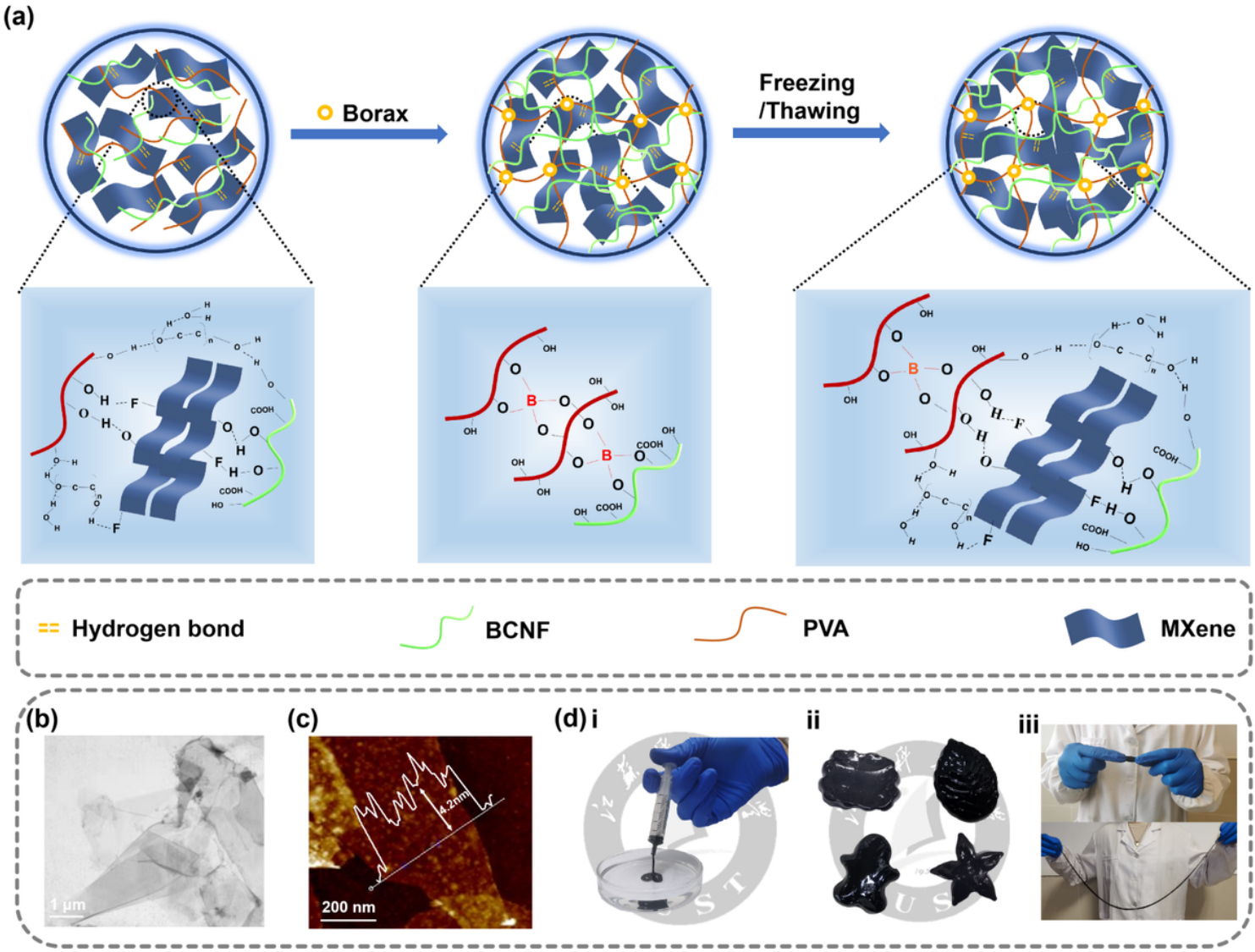

Figure 1

(a) Schematic illustration of the preparation process of MPCB hydrogel; (b) TEM image of MXene; (c) AFM image of MXene nanosheets; (d) Photographs of MPCB samples i) injectability, ii) shapeability, iii) stretchability.

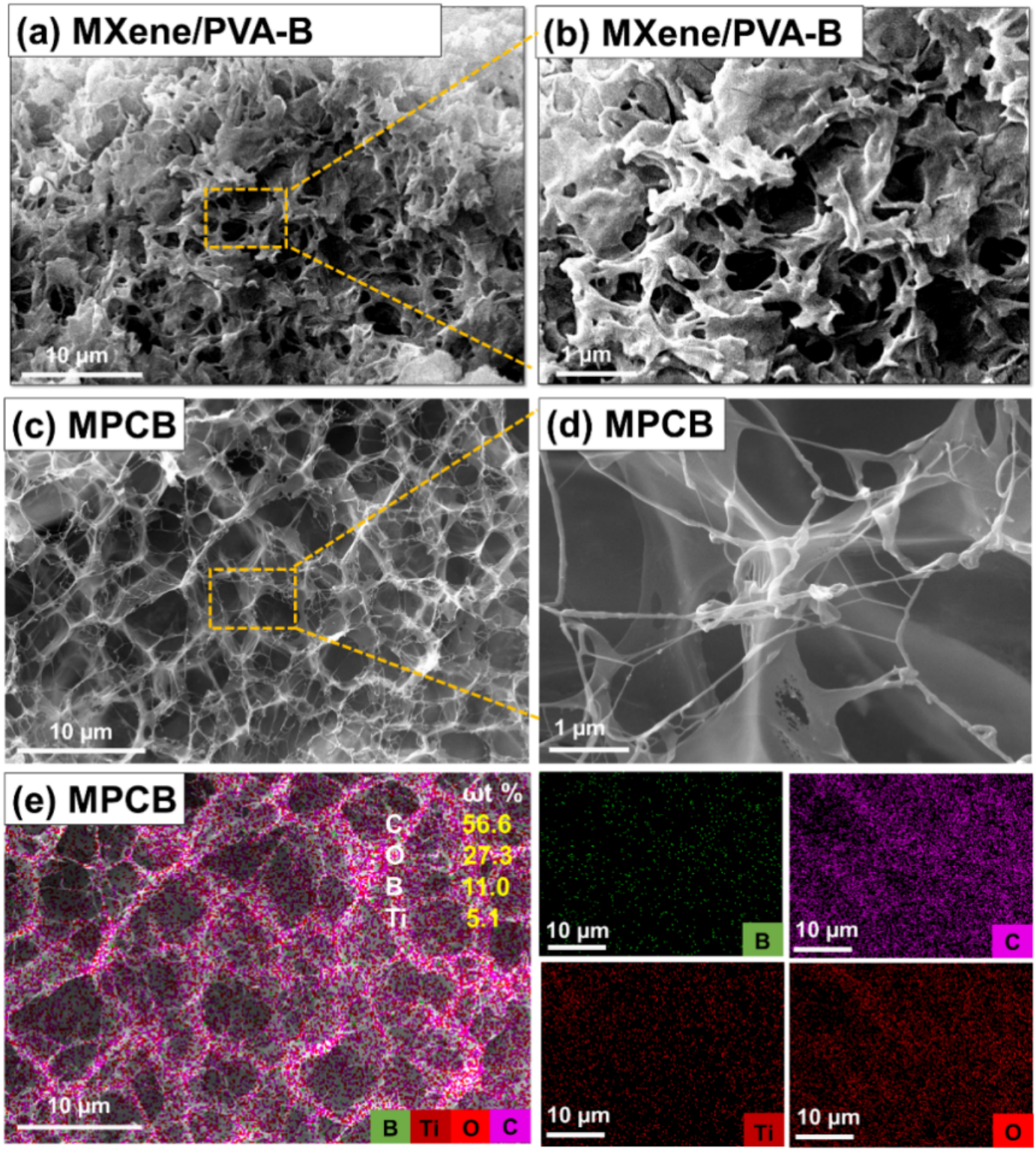

Figure 2

SEM images of (a) MXene/PVA-Bhydrogel and (b) its enlarged detail; (c) MPCB hydrogel and (d) its enlarged details; (e) SEM image and elemental mapping of MPCB hydrogel.

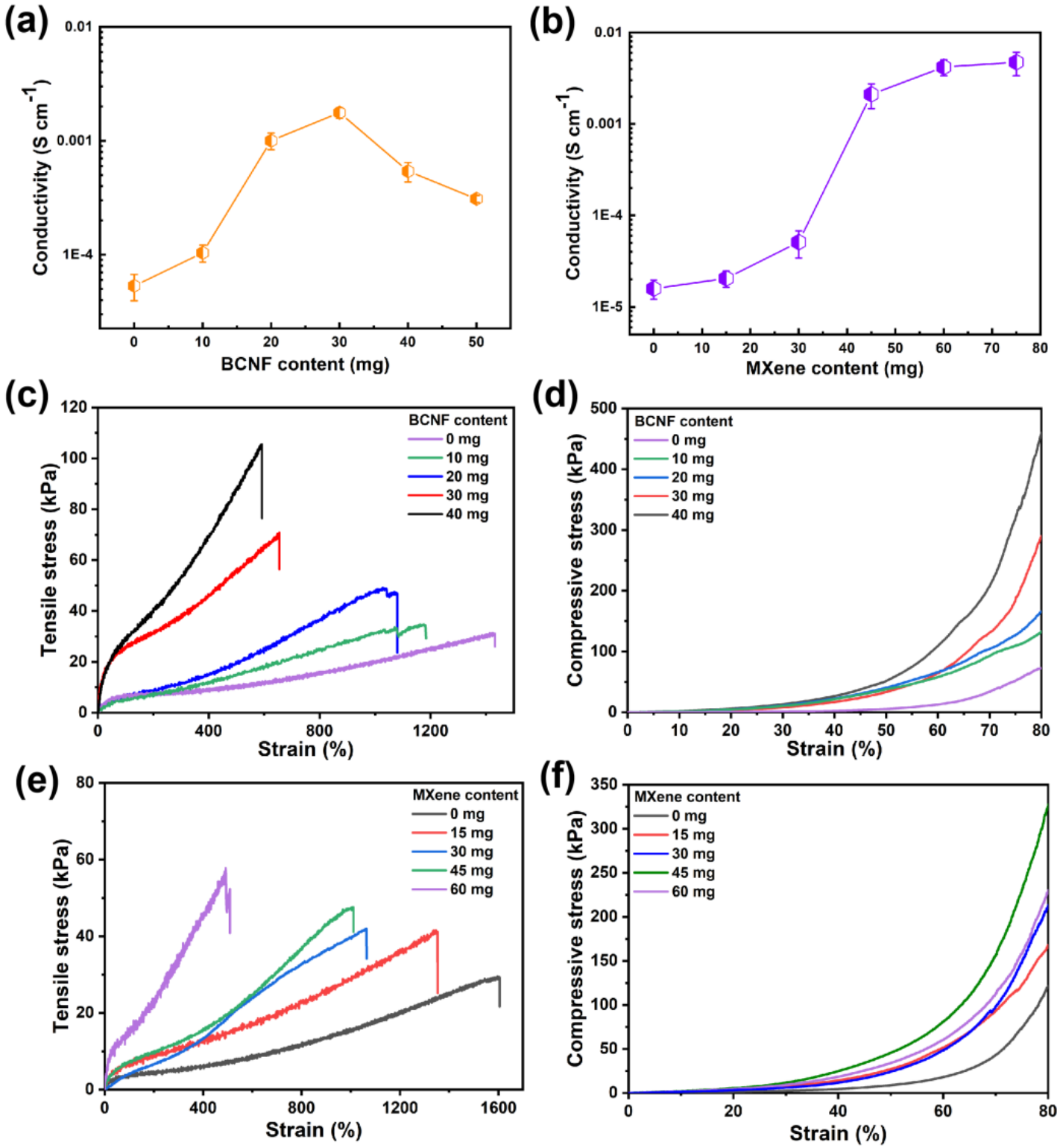

Figure 3

The electrical conductivities of MPCB hydrogels under different (a) BCNF and (b) MXene content; (c) tensile strain curves and (d) compression strain curves of MPCB composite hydrogels under different BCNF content; (e) tensile strain curves and (f) compression strain curves of MPCB composite hydrogels under different MXene content.

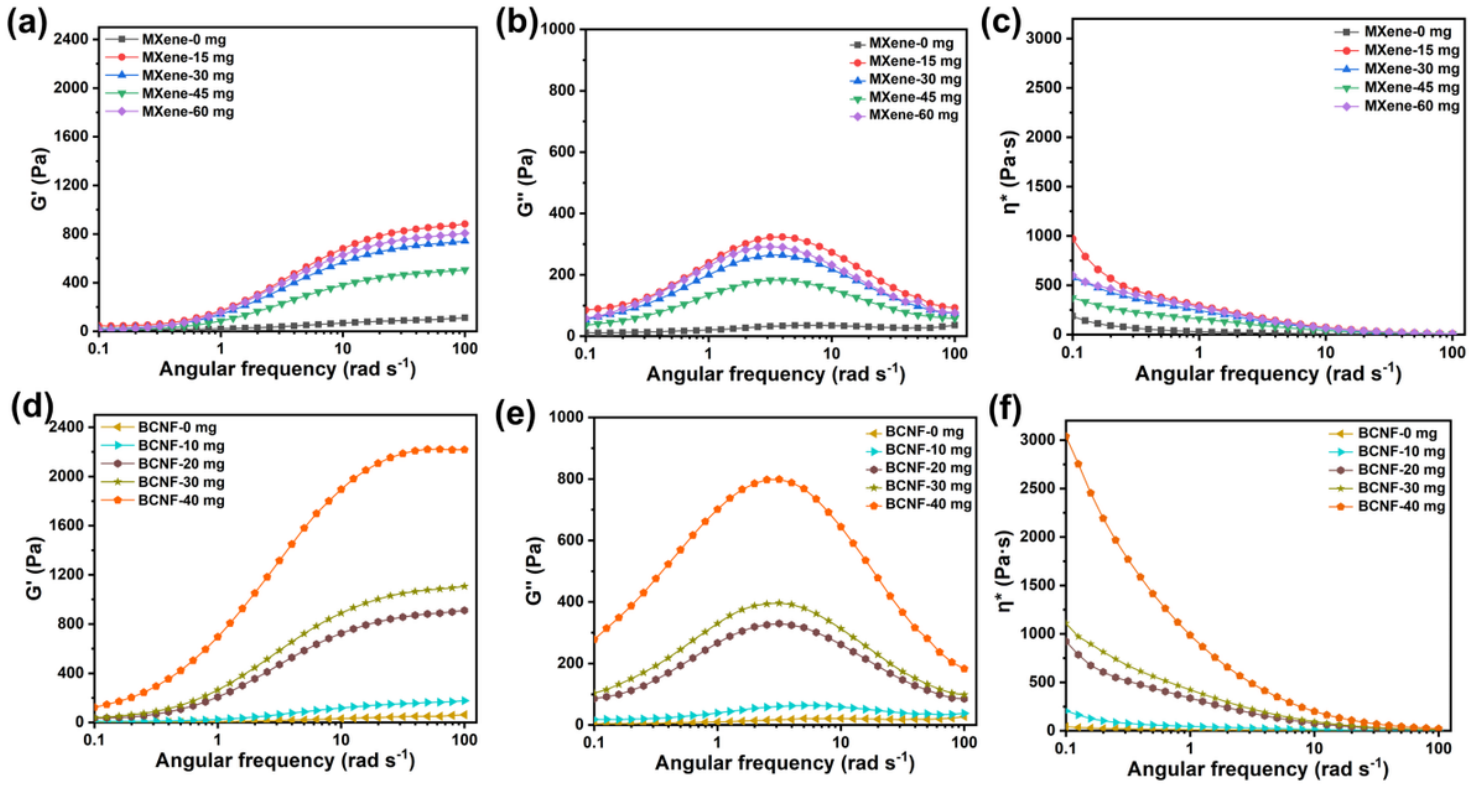

Figure 4

Dynamic viscoelasticity performance of hydrogels: Angular frequency dependence of G', G", and η* of the prepared hydrogels with different content of (a-c) MXene and (d-f) BCNF.

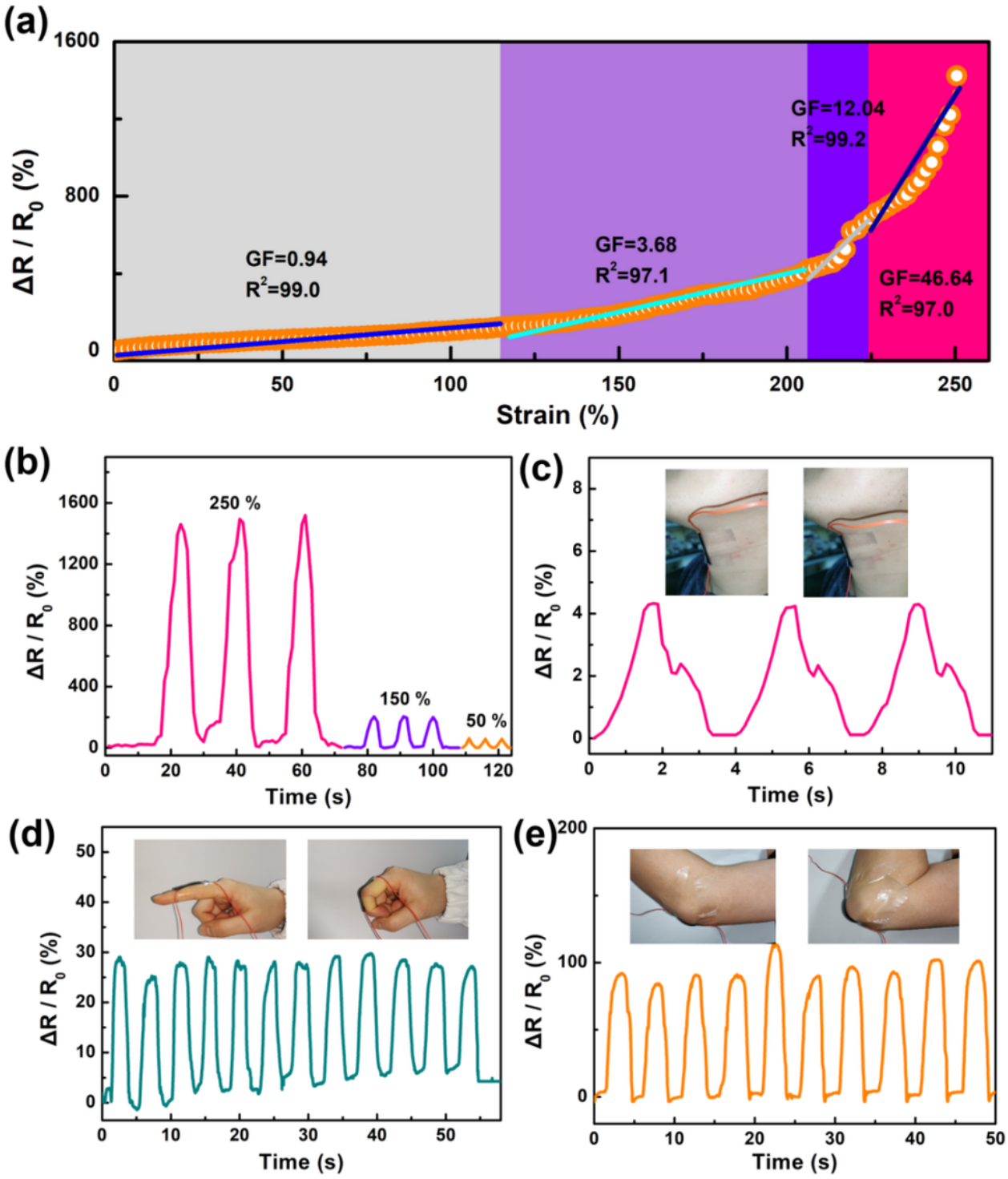

Figure 5

(a) Detailed GF and strain sensing behavior of the MPCB hydrogel; (b) Relative resistance changes under various cyclical maximum strains (250, 150 and 50%) for the MPCB hydrogel; Strain sensing behavior of the MPCB based strain sensor under (c) Adam's apple motion, (d) finger motion and (e) elbow bending.

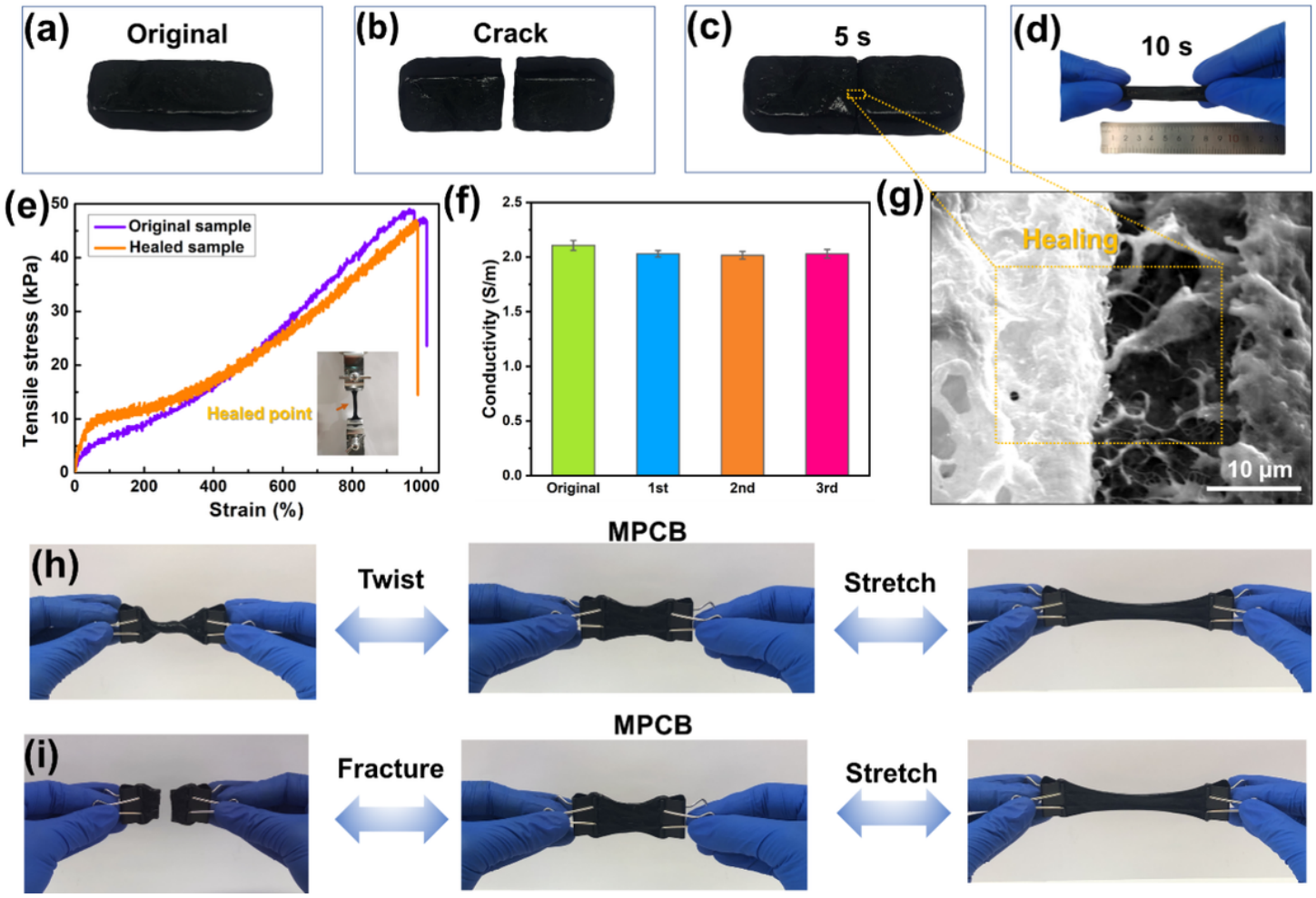

Figure 6

MPCB hydrogel (a) in initial stage, (b) after being cracked, (c) after 5s of rebonding and (d) after 10 s of rebonding; (e) Tensile strain curves of original and healed MPCB hydrogels; (f) The conductivity of the hydrogel after each cutting/healing process; (g) SEM enlarged image of the edge of healed MPCB hydrogel; (h,i) Digital photograph of MPCB hydrogel after twisting and fracture, showing the excellent plasticity and self-healing ability of MPCB hydrogel.

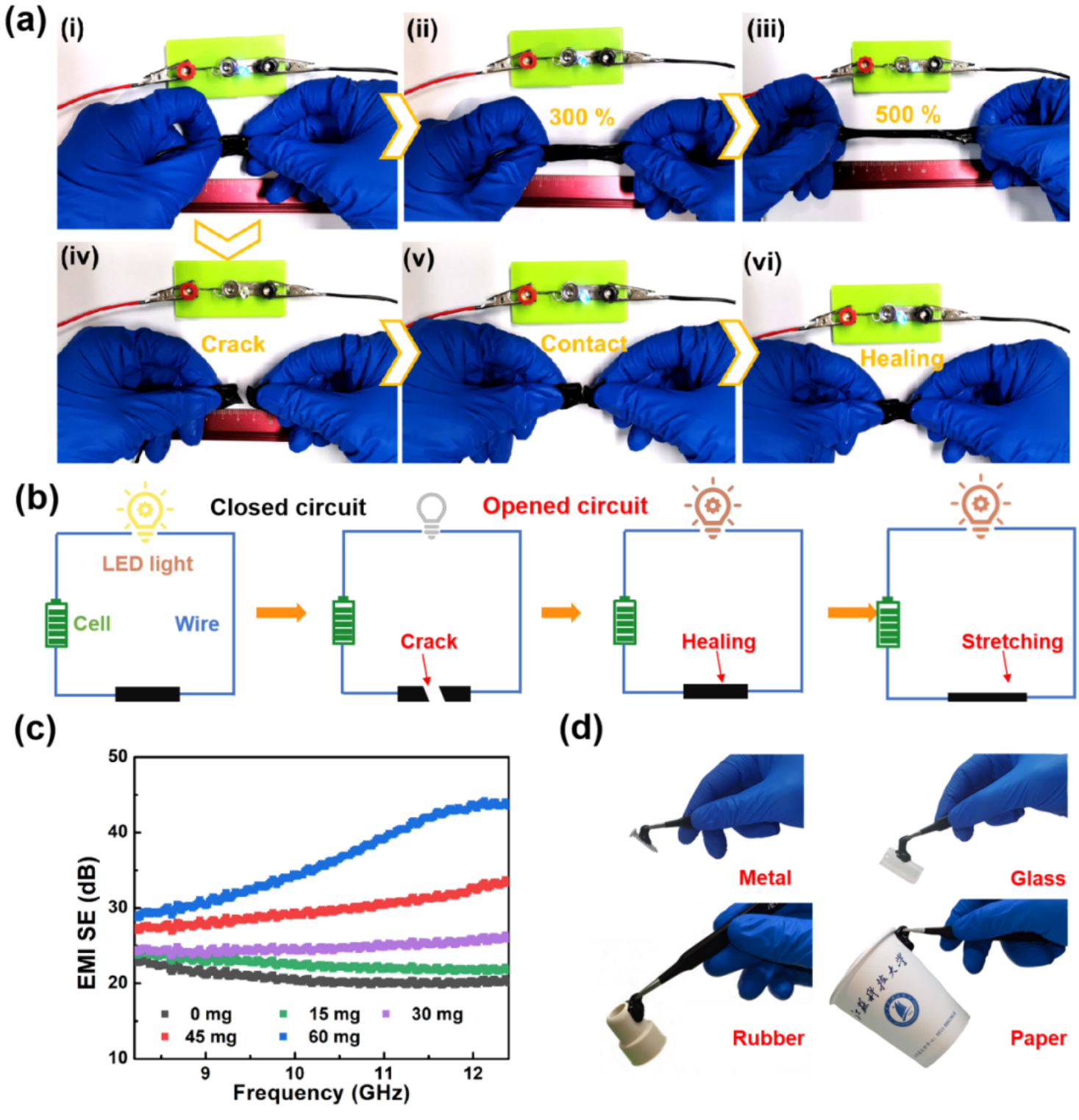

Figure 7

(a) Diagram of conductivity of MPCB hydrogel under different states; (b) the corresponding schematic diagrams of the circuit during the healing process; (c) EMI shielding efficiency of MPCB hydrogels at different content of MXene; (d) Adhesive performance of the MPCB hydrogel to various substrate surfaces: metal, glass, rubber and paper.

Supplementary Files

This is a list of supplementary files associated with this preprint. Click to download.

- Slvs1.0.docx